ORIGINAL ARTICLE

Simulative investigation of the required level of geometrical individualization of the lumbar spines to predict fractures

Laura Kathrin Rieger[1,2] · Mirko Junge[2] · Rachel Cutlan[4] · Steffen Peldschus[1] · Brian D. Stemper[3,4,5]

Abstract

Injury mechanisms of the lumbar spine under dynamic loading are dependent on spine curvature and anatomical variation. Impact simulation with finite element (FE) models can assist the reconstruction and prediction of injuries. The objective of this study was to determine which level of individualization of a baseline FE lumbar spine model is necessary to replicate experimental responses and fracture locations in a dynamic experiment.

Experimental X-rays from 26 dynamic drop tower tests were used to create three configurations of a lumbar spine model (T12 to L5): baseline, with aligned vertebrae (positioned), and with aligned and morphed vertebrae (morphed). Each model was simulated with the corresponding loading and boundary conditions from dynamic lumbar spine experiments. Force, moment, and kinematic responses were compared to the experimental data. Cosine similarity was computed to assess how well simulation responses match the experimental data. The pressure distribution within the vertebrae was used to compare fracture risk and fracture location between the different models.

The positioned models replicated the injured spinal level and the fracture patterns quite well, though the morphed models provided slightly more accuracy. However, for impact reconstruction or injury prediction, the authors recommend pure positioning for whole-body models, as the gain in accuracy was relatively small, while the morphing modifications of the model require considerably higher efforts. These results improve the understanding of the application of human body models to investigate lumbar injury mechanisms with FE models.

Keywords Vertebral body fracture · Individualization · Spinal geometry · FEM · Lumbar spine · Drop test

✉ Laura Kathrin Rieger
laura.rieger@med.uni-munechen.de;
laura.rieger@volkswagen.de

1   Biomechanics and Accident Analysis, Ludwig-Maximilians-Universität (LMU), Occupant Protection System & Virtual Function Development, Volkswagen AG, Letter Box 011/1606 Wolfsburg, Munich 38436, Germany

2   Volkswagen AG, Wolfsburg, Germany

3   Department of Neurosurgery, Medical College of Wisconsin, Milwaukee, WI, USA

4   Department of Biomedical Engineering, Marquette University and Medical College of Wisconsin, Milwaukee, WI, USA

5   Neuroscience Research, Clement J. Zablocki Veterans Affairs Medical Center, Milwaukee, WI, USA

Introduction

Thoracic spine and lumbar spine injuries account for 79% of all spinal injuries and are usually caused by high-energy trauma, mainly falls (39%), traffic crashes (26.5%), and sports accidents (5.2%) [1]. Analysis of injury and crash databases showed that the incidence of thoracolumbar fractures in motor vehicle crashes (MVCs) increased from 1986 to 2008 as a function of vehicle model (National Automotive Sampling System Crashworthiness Data System (NASS-CDS) [2]), from 1994 to 2002 (Crash Outcome Data Evaluation System data [3]), and from 1996 to 2011 with age and seat belt use (Crash Injury Research and Engineering Network (CIREN) [4]).

There are indications that the number of thoracolumbar fractures will increase due to the increase of non-traditional seating postures with the introduction of highly automated vehicles. A reclined seating position, in particular, is predicted to become more prevalent [5, 6] as the forward

rotation of the upper torso occurs later in the reclined position compared to the upright posture, thus increasing the compression in the lumbar spine. Furthermore, a higher degree of thoracolumbar flexion is also associated with causing fractures [7].

Types of fractures vary from major (burst) compression type, with uniform compression of the vertebral body from posterior to anterior, wedge type where the anterior was more compressed than the posterior, and other types that did not fit either category [2, 4, 8]. Such observation can be expected, as the human spine is unique and complex in structure, characterized by complicated anatomy, inhomogeneous material composition, and non-linear material behavior, exposed to complex loading conditions [9]. These anatomical and material variations, combined with differences in load vector, drive varying injury outcomes in motor vehicle crashes.

Some studies investigated significant uncertainties in material properties, geometric configuration, and loading in biological systems [10]. For example, Putzer et al. [11] studied the influence of defined geometrical variations on physiological lumbar spine loading. They reported vertebral body height, disc height, and curvature of the lumbar spine as important. Meijer et al. [12] investigated the physiological range of geometrical dimensions on the stiffness of a motion segment. In their study, disk height had the most considerable influence.

Many studies on spinal alignment in different postures, inherently dependent on other spinal parameters (e.g., disc height, vertebral wedging), have been reported in medical literature the automotive field. For example, Izumiyama et al. [13] investigated skeletal alignment in an automotive seat and tried to clarify the differentiation by age, gender, and body type. Later, studies investigated the effect of the postural change between standard seating postures and a reclined posture in vehicles [14] and the effect of the seat back inclination on spinal alignments comparing spinal alignments of automotive seating postures in the 20° and 25° seat back angle and standing and supine postures [15].

The depiction of injury mechanisms for injury reconstruction or prediction requires a description of the relevant anatomical details. Therefore, the ultimate aim would be to consider all anatomical and pathological variants of the spine. Human body models (HBMs) are suitable as an evaluation methodology, especially for evaluating different anthropometries. HBMs are computationally efficient, reproducible, and repeatable, though their main advantage lies in individualization. They have been individualized on the full-scale level [16, 17] but also the component level [18, 19].

Individualization of full-scale HBMs can offer realistic occupant populations. Their generation and preparation for application would require a fully automated method to produce many whole-body FE human models representing sexes and a wide range of stature and body shapes, like the mesh morphing method presented by Zhang et al. [16]. They generated 100 human models with a wide range of variation. The main limitation of the study is its focus on statistical models of the ribcage, pelvis, femur, and tibia. At the same time, the other skeletal components were morphed using geometric relationships among the adjacent structures, but without reference to specific skeletal data. Nevertheless, even if it was possible to integrate all feasible spinal characteristics, actual parameters are usually unknown, and variability is inherent in living organisms. Finally, setting up individual-specific models for each spinal curvature is inefficient and not economical. Knowledge about the loss of precision with different simplifications in the individualization approach would be helpful.

Therefore, the objective of this study was to (1) identify the spine parameters in the sagittal plane responsible for kinematic behavior in a dynamic application and (2) propose an application strategy that allows systematic inclusion of variance in the analysis. To the author's knowledge, there are no investigations on the influence of geometrical parameters on the whole lumbar spine in dynamic lumbar spine compression. Hence, a component load case of the complete lumbar spine (T12-L5) by Stemper et al. [20] was used as an experimental validation load case, and the Total Human Model for Safety v4.1 (THUMS v4.1) lumbar spine was used to apply three different individualization levels: The first individualization level was the original (unchanged, baseline) THUMS v4.1 lumbar spine, the second level was created via positioning of the vertebrae according to sagittal imaging data from the experiment, and the third level, the highest level of individualization, included adaption of the height of the vertebral bodies via morphing and positioning of the vertebrae. All different models were assessed in the same load cases concerning global kinetics, vertebrae kinematics, and fracture prediction potential.

Materials and methods

Experiments

The basis for this study is an analytical study with Level of Evidence II by [20] Stemper et al. (2017), in which axial tolerance of 26 lumbar spines (T12-L5) in combined compression and flexion was experimentally quantified using a drop tower test (see Table S1). CT scans and lateral X-rays were obtained of each specimen to confirm spinal integrity (via CT scan) and positioning (via X-ray) before testing. Cranial (T12) and caudal (L5)

vertebrae were embedded in polymethylmethacrylate to facilitate attachment to the experimental apparatus. The L2-L3 disc level was kept approximately horizontal in the global coordinate system without altering the natural specimen-specific lordosis to ensure consistency of pre-load between specimens.

Compressive flexion loading was applied to whole lumbar spine specimens using a drop tower with two decoupled platforms attached to a monorail via low-friction bearings. Each specimen was attached through a load cell to the lower platform, and a laterally oriented cylinder enabled interaction between the decoupled upper platform and the superior specimen fixation. A 5 Nm pre-flexion torque was applied at the superior specimen fixation while minimizing anterior-posterior and lateral shear forces. The specimen was held in that position with the laterally oriented cylinder. The relative position of the two platforms was fixed using a cable that allowed the upper platform to apply inertial compressive loads to the specimen by reducing the vertical distance to the lower platform during deceleration while also preventing specimen recoil before testing and significant vertical displacement or impact during dynamic testing. A 32 kg mass was added to the upper platform to simulate static torso mass of a 50th-percentile male.

At the bottom of the drop tower test setup, a piece of foam was used to form a realistic acceleration pulse. Linear accelerometers were used at the lower and upper platforms to measure vertical accelerations. Forces and moments were measured via a load cell, which was attached at the caudal fixation of the specimen to the lower platform.

Each specimen was exposed to one or more dynamic tests from specific drop heights until an injury was detected. An incremental paradigm was used, wherein drop heights were increased after non-injury tests. A Vicon system (Vicon Corp., Oxford Metrics Group, Oxford, England) with three spherical targets (one target placed in the anterior aspect of the body and one in each transverse process) was used to record three-dimensional vertebral kinematics. Local cartesian coordinate system origins were defined at mid-height and mid-width along the posterior wall of each vertebral body. Vertebral kinematics were reconstructed by using target motions. Sagittal segmental angulation was computed for each segment (T12-L1 through L4-L5) as the sagittal plane angle of one vertebra relative to the subjacent vertebra [20].

After each test, specimens were examined for fractures and abnormal changes in spinal alignment or disc heights using X-rays. Specimen palpation and flexion stiffness assessments excluded endplate or soft tissue injury. Testing of a specimen was immediately stopped when an injury was detected. Fracture classification and the affected spinal level were assessed using X-rays and post-test CT scans.

Simulation

Development of FE models

The THUMS (v4.1) lumbar spine for T12 to L5 with ligaments and intervertebral discs was selected for simulations. The material properties of the annulus fibrosus and the capsular ligament have been adapted according to data from the literature [21–23]. Local coordinate systems (LCS) have been defined for each vertebral body according to a previously published method [24].

The LCS were tied to and moved in conjunction with their respective vertebrae for the duration of each test, allowing for comparison with the PHMS experiment. All simulations were conducted in Visual-Crash PAM (ESI Group, Rungis, France).

The 26 different samples were simulated in three different configurations, i.e., in the *original* or *baseline* THUMS position, in a *positioned*, and a *morphed* version, resulting in a total of 78 simulations. For the morphed configuration, pretest midsagittal X-ray images were used to determine the anterior and posterior heights of the vertebral bodies and the anterior and posterior heights of the intervertebral discs. Following previous investigations on spinal segmental kinematics, angles [25–30, 15] were measured using the image processing software ImageJ for the positioned and the morphed configuration (http://rsb.info.nih.gov/ij/; US National Institutes of Health Bethesda, Maryland, USA).

No geometrical adaptations on the THUMS lumbar spine unit were made for the baseline configuration. The changes to the segmental angles were applied to place the model for the positioned configuration. For the morphed configuration, the lateral heights of the vertebral bodies were individualized using DFM morphing in ANSA (BETA CAE Systems SA, Epanomi, Thessaloniki). After adaption of the heights, the articulation tool for human body model positioning available in ANSA was used to position the models according to the intervertebral angles measured in the X-rays (see Fig. 1).

Boundary and loading conditions

A simplified setup of the drop tower apparatus was implemented while maintaining the boundary conditions to compare the simulations to previous PHMS experiments. The THUMS lumbar spine unit was rotated for the baseline configuration to keep the L2-L3 disc level approximately horizontal in the global coordinate system.

To globally position the positioned and the morphed configuration, the distance of the lower potting to L5 in x- and z-direction and the tilt angle of L5 to the global x-axis in the X-rays were measured. The height and the tilt of the
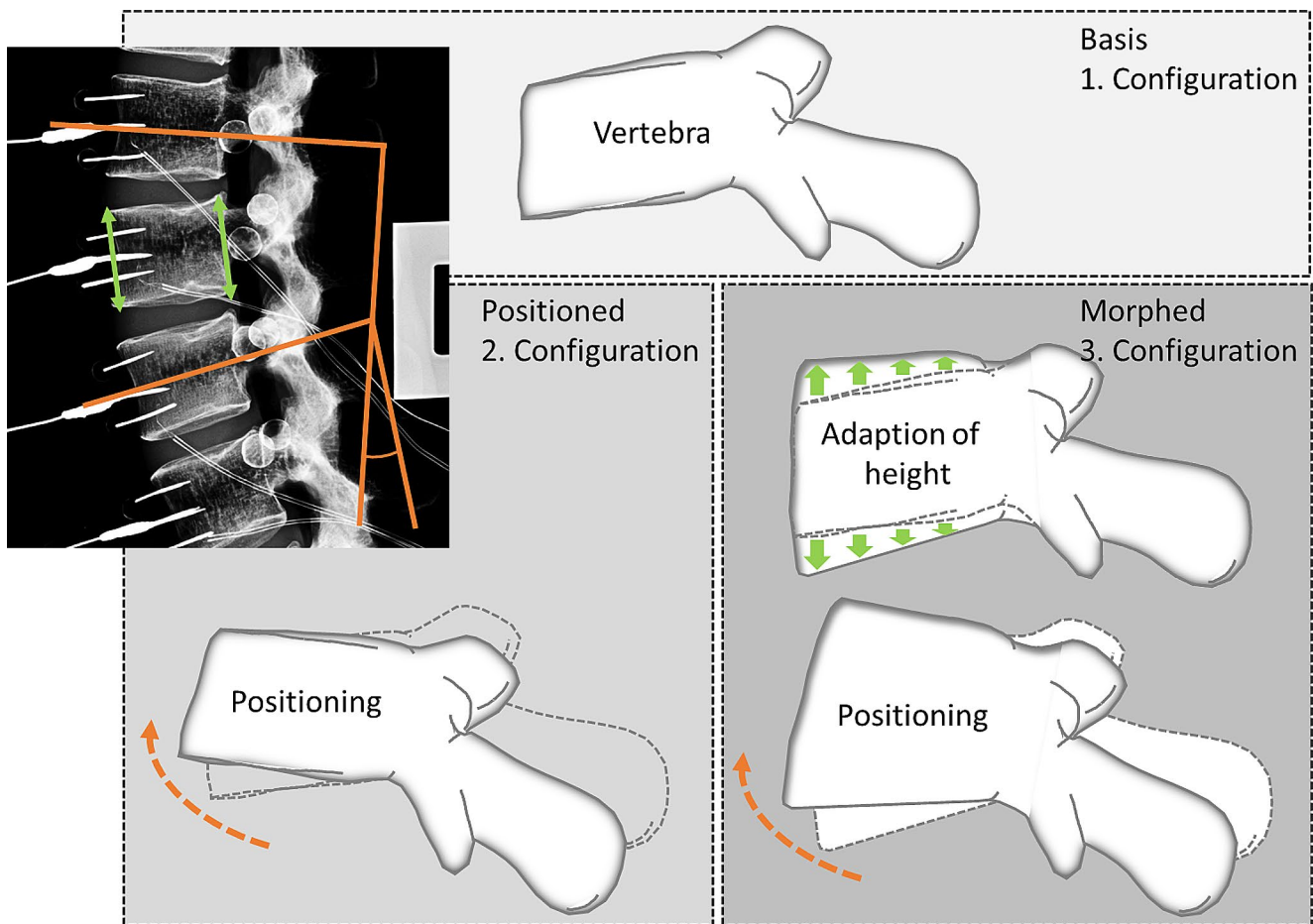
Fig. 1 Modelling approach for the three different lumbar spine configurations – morphed (3. Configuration), positioned (2. Configuration) and baseline (1. Configuration) – exemplarily shown on one vertebra

upper potting, as well as the position of the impactor with a non-structural mass of 32 kg, were individualized for each specimen according to the pretest X-rays. Then, the superior (T12) and inferior (L5) vertebrae were positioned in finite element models of aluminum potting cups, bone cement-like potting resin, and aluminum load cells used in the experiments.

The vertebrae's superior and inferior cortical shells were rigidly fixed to the deformable potting resin, and the potting resin was constrained to the rigid potting cups. Afterward, the upper potting was translated in z-direction to the same position on the cranial end of the LSUs as shown in the X-rays.

A frictionless self-contact was implemented to allow relative movement between the upper potting and the impactor. To limit the movement of the impactor in z-direction in the rebound phase, as was ensured by the cable in the experiments, a plate was added on top. To mimic the drop tower setup's release of boundary conditions, the cylinder and the lower platform allow translation in global z-direction and around global y-axis. Simulation responses were compared to PHMS kinetic and kinematic responses: section forces in the upper and lower specimen pot enable measuring of section forces in the global coordinate system.

The accelerations measured in the experiment in the lower platform are applied as input to the lower specimen pot below the section force to allow for accurate measurement. In addition to the forces and moments as measured in the specimen experiments, intervertebral kinematics were also measured in the simulation. Gravity was applied to the whole setup as an acceleration field. (see Fig. S1)

Model evaluation

The modified THUMS models were evaluated relative to the specimen test data by comparing the kinetics (forces and moments measured at the caudal end) and vertebral kinematics. In the experiments, target motions were used to reconstruct vertebral kinematics, and sagittal segmental angulation was computed for each segment (T12-L1 through L4-L5).

A similar approach to analyzing vertebral kinematics was performed in this study on the simulation data. Local coordinate systems defined in each vertebral body were used to calculate sagittal vertebral angles. For calculating the sign of the angles (negative - extension, positive - flexion) a plane was defined that spans each two local x-vectors in the sagittal plane. The sign of the resulting vector product between the two local x-vectors then determines the opening of the angle.

The similarity of the outputs of the simulation and the experimental results were analyzed until time of peak force was reached; it was assessed using the *cosine similarity* function in MATLAB (R2020a, The MathWorks, Inc., Natick, MA, USA). The closer the cosine similarity value is to 1, the smaller the cosine angle and the greater the match between vectors. Cosine similarity can be used as measure for numeric data that ignores zero-matches [31]. Here, the cosine similarity analysis was applied for each scalar (force or moment component) in the time diagram. The cosine value was also used to rate the simulation configurations for each specimen.

Vertebrae injury predictors

To identify the mechanism of vertebral compression fracture, the pressure (precisely, negative one third of the first invariant or trace of the stress tensor) of the spongiosa was analyzed. This analysis was performed by finding the peak pressure in each vertebra before the time of peak force is reached. Therefore, the maximal and minimal values of the scale of the contour plots of the models were set to the same overall maximal and minimal values. The contour plots were then filtered until only the elements exceeding a threshold were shown, which would then also define a potential fracture region.

Results

The experimental data of 26 PHMS from which lumbar spine data was obtained were used for simulation. Eleven of the 26 PHMS lumbar spines were from female donors, thirteen were from male donors, and for two, sex, mean age, height, and weight were unknown. The mean age, height, and weight of the female PHMS were 48 ± 12 yrs., 161 ± 11 cm, and 68 ± 19 kg, for the male PHMS 44 ± 12 yrs., 177 ± 6 cm, and 80 ± 11 kg, respectively. Experimental data of each specimen was used for the simulative setup of the baseline, positioned, or morphed configurations.

FE model validation

Global kinetic evaluation

Figure 2 shows the kinetic response of one specimen in all different configurations, i.e., baseline, positioned, and morphed. Compared to all other responses axes, the amplitude of z-force and y-moment is significantly higher; the primary focus is evaluating these responses.

For the *baseline* configuration, the kinetic model responses for z-force und y-moment were opposite to the experimental responses in half of the cases; for the other half, one of the responses was off in the opposite direction. For fourteen cases, the cosine value for the z-force responses of the baseline THUMS configuration is greater than 0.8, eight cases are between 0.5 and 0.8, and all other cases are less than 0.5. At the same time, for the y-moment, it is less than 0.8 for twenty-four cases and between 0.5 and 0.8 for five cases (see Fig. 3).

For the *positioned* configuration, in seven cases (27%), one model response was opposite to the experimental curves; for one case, none aligned with the experimental responses. The response aligned with the experimental responses for all other cases (77%). The cosine value for the z-force is in twenty-three cases greater than 0.5 and twenty-four cases greater than 0.8. For the y-moment in twelve cases, the z-force is greater than 0.5, and one specimen's response has a cosine value greater than 0.8. All other remaining responses are less than 0.5 (see Fig. 3).

Regarding the configuration with the *morphed* sagittal vertebral body heights, intervertebral discs, and positioned vertebrae, fifteen cases (58%) of all specimen's responses followed the same trend as the experimental responses - at least one of the responses aligned with the trend for twenty-one cases. The cosine value for the z-force was greater than 0.8 for nineteen cases and was between 0.5 and 0.8 for three cases. For the y-moment, eleven cases showed a cosine value greater than 0.8, and two, cosine values were between 0.5 and 0.8. The cosine values for the responses of the thirteen remaining specimens were lower than 0.5 (see Fig. 3).

Kinematic evaluation at vertebra level

Figure 4 shows the intervertebral kinematics per vertebra segment over time for one specimen across all configurations. The time history of these plots was used to calculate the cosine value for each curve. The results are listed in Fig. 5. For the *baseline* configuration, more than 10 to 22 specimen cases show a similarity value of less than 0.5, and 15 to 23 cases show at least a similarity value less than 0.8. The *positioned* configurations show similarity values less than 0.5 in 7 to 17 cases and less than 0.8 in 12 to 22 cases.
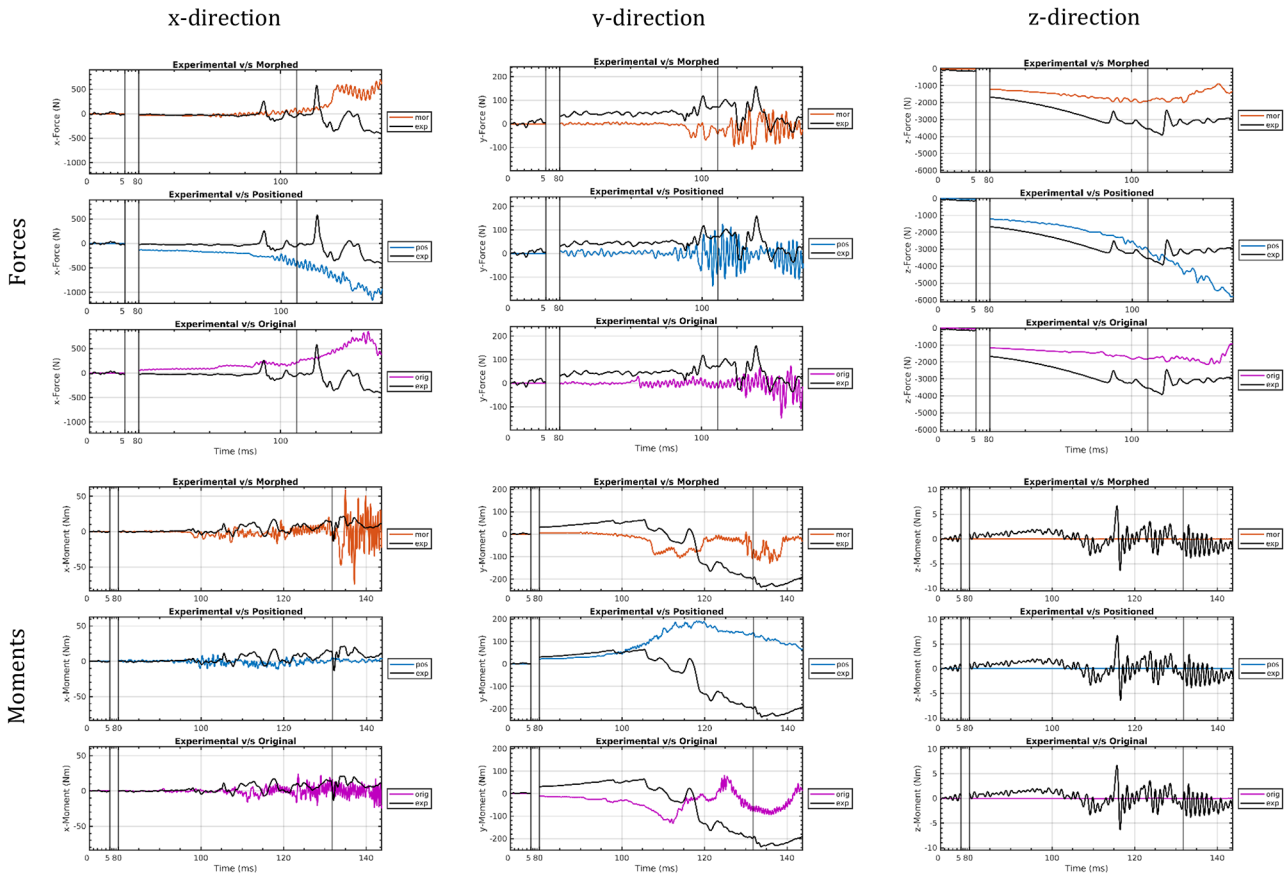
x-direction   y-direction   z-direction

Forces

Moments

Fig. 2 THUMS simulation **kinetic** response (top – force, bottom - moment) in three different configurations compared to PMHS exemplarily for one specimen. THUMS curves are plotted starting at 80ms and for the duration of the simulation. Plots of other specimens can be found in the Supplementary Material

Specimens	x-Force			y-Force			z-Force			x-Moment			y-Moment			z-Moment		
	morphed	positioned	original	morphed	positioned	original	morphed	positioned	original	morphed	positioned	original	morphed	positioned	original	morphed	positioned	original
1	0.93146	0.91409	-0.79021	-0.37436	-0.053258	-0.011885	0.92083	0.9689	0.9395	0.15502	-0.049352	-0.11147	0.98904	0.99498	-0.96353	-0.7318	-0.7443	0.73952
2	0.16251	0.42267	-0.38891	-0.41253	0.035478	-0.057397	0.9724	0.97979	0.96945	-0.072318	-0.24875	0.045068	0.47576	-0.51523	0.053467	0.17657	-0.034114	0.23523
3	0.97329	0.96136	-0.92298	-0.049344	-0.18473	-0.071753	0.89501	0.96592	0.90088	-0.0003034	0.29831	-0.000474	0.95671	0.98759	-0.96888	0.065731	0.10537	0.068747
4	0.9584	0.99262	-0.92518	-0.74751	-0.011102	-0.23389	0.88884	0.95556	0.91828	-0.61925	-0.51106	-0.12641	0.84363	0.9795	-0.43832		-0.91229	0.089188
5	0.83238	0.82422	-0.70552	-0.0069264	0.11618	0.26686	0.99043	0.99527	0.98009	0.17577	0.46854	0.34734	0.51403	0.46812	-0.31808	-0.009023	0.077959	-0.43821
6	0.92998	0.90629	-0.83341	-0.089038	-0.49748	-0.64359	0.95998	0.98554	0.98151	0.057359	0.27089	0.4005	0.95541	0.92257	-0.60076	0.49018	0.44212	0.19912
7	-0.44825	-0.44488	0.58009	-0.094221	0.14368	-0.16356	0.36768	0.26581	0.33284	0.13683	0.0039214	-0.057551	0.33078	0.41163	-0.31164	0.11829	0.043977	-0.045798
8	-0.51095	-0.6122	-0.61882	-0.22358	0.13141	0.14532	0.49479	0.50942	0.43768	0.37363	-0.16814	-0.28175	0.35093	0.34184	0.64011	-0.0075177	-0.0010056	
9	0.96163	0.96301	-0.40419	-0.084708	0.23362	0.12797	0.97234	0.98918	0.60039	0.0049076	-0.32775	-0.2912	-0.78169	-0.75198	0.43384	-0.092008	0.0074712	
10	-0.18258	-0.56886	-0.68512	0.042082	0.043689	0.29491	0.75575	0.91585	0.63116	0.060419	-0.29836	0.12841	-0.41656	-0.76626	-0.85417	0.096826	-0.032086	0.020734
11	-0.17058	-0.024788	-0.35332	-0.047316	-0.096427	-0.11478	0.6565	0.44934	0.78818	0.1331	0.26724	0.34547	0.21862	-0.3449	0.43633	0.28091		
12	0.736	0.79497	0.32653	0.33397	0.037712	0.18115	0.94552	0.97449	0.91985	-0.47806	0.19013	-0.57951	0.81534	0.92375	0.28327	0.29029	-0.28132	0.1835
13	-0.64159	-0.79221	-0.93635	-0.0037063	-0.03961	0.17306	0.91441	0.91901	0.81736	-0.22502	0.080594	0.6088	0.53783	0.73616	0.96629	-0.26313	0.36133	0.36239
14	0.98995	0.98457	-0.19874	-0.35577	-0.79056	-0.20263	0.88728	0.92753	0.43371	0.63615	0.61233	0.33008	0.91194	0.89092	-0.49216	0.5855	0.67086	-0.14333
15	0.9727	0.97452	-0.76256	0.020963	0.13971	0.11804	0.9083	0.98407	0.51774	-0.55757	-0.62917	-0.16719	0.9648	0.98362	-0.18742	-0.51856	-0.89938	-0.41665
16	0.97883	0.98783	-0.97244	-0.13606	0.095016	0.099267	0.8556	0.93079	0.96527	0.39295	0.62651	0.23346	-0.76616	-0.785	0.22173	-0.0065322	0.44824	-0.49662
17	0.9783	0.99172	-0.9728	0.040047	0.062999	0.32934	0.93723	0.9693	0.91718	-0.2082	-0.51384	-0.57596	0.99403	0.99476	-0.90997	0.13125	-0.092261	0.29031
18	0.98557	0.9896	-0.88125	-0.067905	0.15163	-0.51993	0.96912	0.98307	0.95556	0.030097	-0.16174	0.44556	0.98179	0.97211	-0.9582	0.77243	0.8716	-0.53277
19	0.92607	0.95731	-0.081898	0.032302	-0.029239	-0.12089	0.98615	0.99102	0.56847	-0.10544	0.041524	0.24226	0.96466	0.96334	-0.3751	0.77611	0.75787	-0.16133
20	0.98856	0.97531	-0.89796	-0.051431	-0.069999	-0.10235	0.93565	0.97576	0.95256	0.44516	0.47423	0.32551	0.98119	0.9788	-0.90823	0.45107	0.82088	-0.33125
21	-0.50673	0.50477	-0.95376	-0.12216	-0.23932	-0.22426	0.9124	0.96671	0.91598	0.16916	0.27005	0.58674	-0.18681	-0.065637	-0.72117	-0.35568	-0.14447	0.059071
22	0.94851	0.98187	-0.73196	0.011769	0.23491	-0.029811	0.95596	0.99501	0.59283	0.039636	0.069435	0.03329	-0.53053	-0.748	0.61333	-0.029725	0.25548	-0.087507
23	-0.88642	-0.50499	-0.8202	0.50616	0.35518	0.65403	0.95376	0.96709	0.93485	-0.34903	-0.2393	-0.5731	0.34437	0.34798	-0.13988	-0.033333	-0.046764	0.21732
24	0.94904	0.96804	-0.82406	-0.64733	-0.56227	-0.1599	0.78337	0.84968	0.47008	0.28642	0.32731	0.25265	-0.77927	-0.79794	0.65802	-0.26006	-0.092467	
25	-0.96334	-0.95117	-0.90719	-0.17723	-0.17215	-0.10005	0.94818	0.96505	0.76587	-0.033473	-0.11365	0.1061	0.4562	0.52513	0.8042	-0.15194	0.088459	-0.78146
26	-0.69801	-0.8889	-0.78221	-0.13165	-0.28489	-0.10655	0.46	0.84909	0.5321	-0.059718	-0.081379	0.012967	0.28901	0.074014	0.49476	0.0020605	0.0067807	

Cosine value
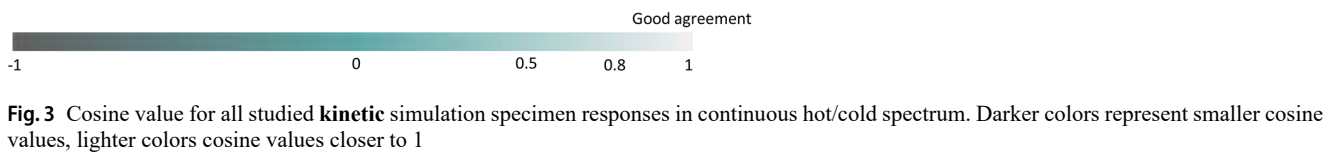
Good agreement

-1   0   0.5   0.8   1

Fig. 3 Cosine value for all studied **kinetic** simulation specimen responses in continuous hot/cold spectrum. Darker colors represent smaller cosine values, lighter colors cosine values closer to 1

Fig. 4 THUMS simulation **kinematic** response in four different configurations (morphed, positioned, baseline) compared to PHMS exemplarily for one specimen. THUMS curves are plotted for the duration of the simulation. Plots of other specimens can be found in the Supplementary Material
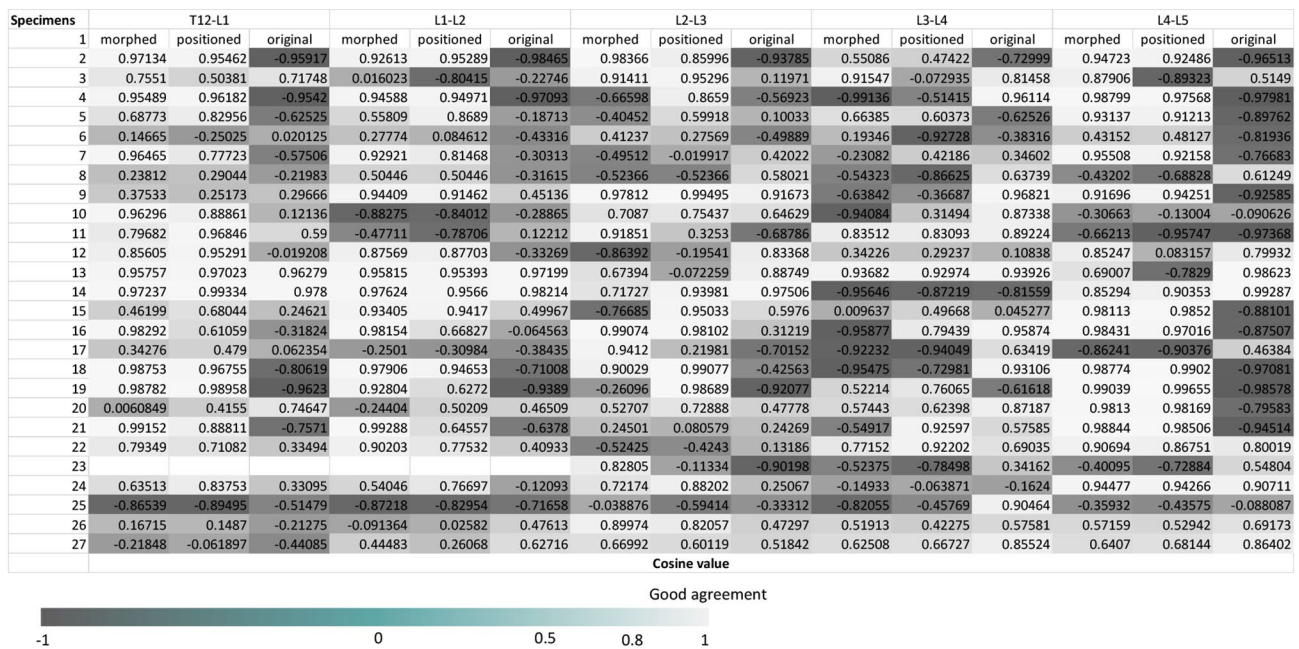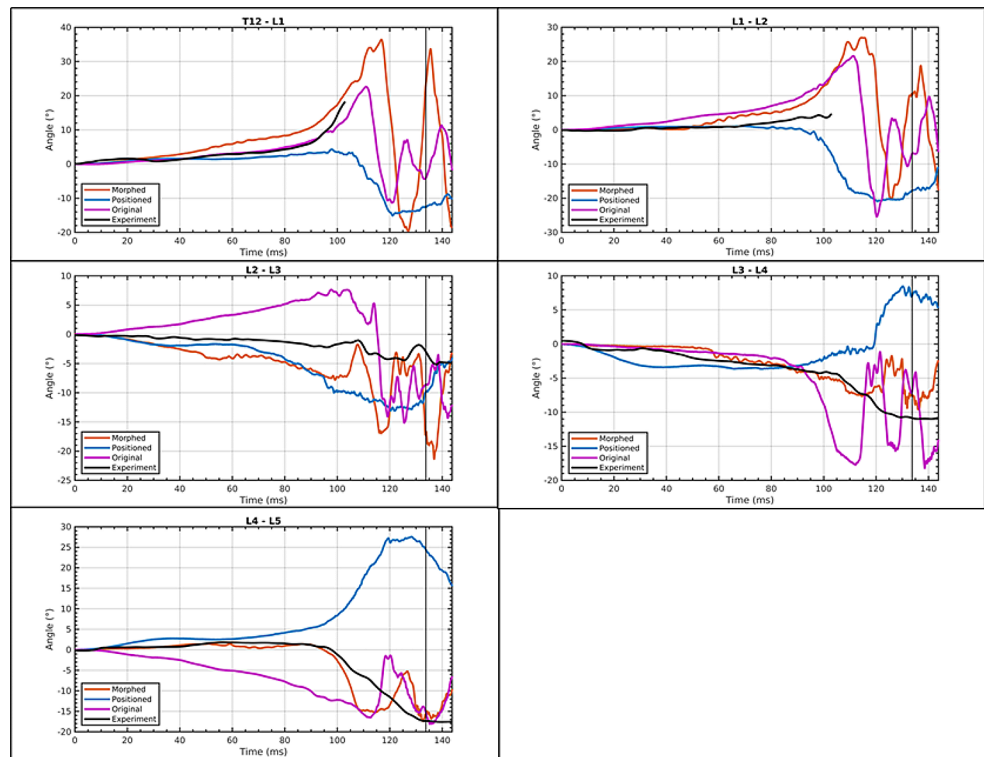

Specimens	T12-L1			L1-L2			L2-L3			L3-L4			L4-L5		
1	morphed	positioned	original	morphed	positioned	original	morphed	positioned	original	morphed	positioned	original	morphed	positioned	original
2	0.97134	0.95462	-0.95917	0.92613	0.95289	-0.98465	0.98366	0.85996	-0.93785	0.55086	0.47422	-0.72999	0.94723	0.92486	-0.96513
3	0.7551	0.50381	0.71748	0.016023	-0.80415	-0.22746	0.91411	0.95296	0.11971	0.91547	-0.072935	0.81458	0.87906	-0.89323	0.5149
4	0.95489	0.96182	-0.9542	0.94588	0.94971	-0.97093	-0.66598	0.8659	-0.56923	-0.99136	-0.51415	0.96114	0.98799	0.97568	-0.97981
5	0.68773	0.82956	-0.62525	0.55809	0.8689	-0.18713	-0.40452	0.59918	0.10033	0.66385	0.60373	-0.62526	0.93137	0.91213	-0.89762
6	0.14665	-0.25025	0.020125	0.27774	0.084612	-0.43316	0.41237	0.27569	-0.49889	0.19346	-0.92728	-0.38316	0.43152	0.48127	-0.81936
7	0.96465	0.77723	-0.57506	0.92921	0.81468	-0.30313	-0.49512	-0.019677	0.42022	-0.23082	0.42186	0.34602	0.95508	0.92158	-0.76683
8	0.23812	0.29044	-0.21983	0.50446	0.50446	-0.31615	-0.52366	-0.52366	0.58021	-0.54323	-0.86625	0.63739	-0.43202	-0.68828	0.61249
9	0.37533	0.25173	0.29666	0.94409	0.91462	0.45136	0.97812	0.99495	0.91673	-0.63842	-0.36687	0.96821	0.91696	0.94251	-0.92585
10	0.96296	0.88861	0.12136	-0.88275	-0.84012	-0.28865	0.7087	0.75437	0.64629	-0.94084	0.31494	0.87338	-0.30663	-0.13004	-0.090626
11	0.79682	0.96846	0.59	-0.47711	-0.78706	0.12212	0.91851	0.3253	-0.68786	0.83512	0.83093	0.89224	-0.66213	-0.95747	-0.97368
12	0.85605	0.95291	-0.019208	0.87569	0.87703	-0.33269	-0.86392	-0.19541	0.83368	0.34226	0.29237	0.10838	0.85247	0.083157	0.79932
13	0.95757	0.97023	0.96279	0.95815	0.95393	0.97199	0.67394	-0.072259	0.88749	0.93682	0.92974	0.93926	0.69007	-0.7829	0.98623
14	0.97237	0.99334	0.978	0.97624	0.9566	0.98214	0.71727	0.93981	0.97506	-0.95646	-0.87219	-0.81559	0.85294	0.90353	0.99287
15	0.46199	0.68044	0.24621	0.93405	0.9417	0.49967	-0.76685	0.95033	0.5976	0.009637	0.49668	0.045277	0.98113	0.9852	-0.88101
16	0.98292	0.61059	-0.31824	0.98154	0.66827	-0.064563	0.99074	0.98102	0.31219	-0.95877	0.79439	0.95874	0.98431	0.97016	-0.87507
17	0.34276	0.479	0.062354	-0.2501	-0.30984	-0.38435	0.9412	0.21981	-0.70152	-0.92232	-0.94049	0.63419	-0.86241	-0.90376	0.46384
18	0.98753	0.96755	-0.80619	0.97906	0.94653	-0.71008	0.90029	0.99077	-0.42563	-0.95475	-0.72981	0.93106	0.98774	0.9902	-0.97081
19	0.98782	0.98958	-0.9623	0.92804	0.6272	-0.9389	-0.26096	0.98689	-0.92077	0.52214	0.76065	-0.61618	0.99039	0.99655	-0.98578
20	0.0060849	0.4155	0.74647	-0.24404	0.50209	0.46509	0.52707	0.72888	0.47778	0.57443	0.62398	0.87187	0.9813	0.98169	-0.79583
21	0.99152	0.88811	-0.7571	0.99288	0.64557	-0.6378	0.24501	0.080579	0.24269	-0.54917	0.92597	0.57585	0.98844	0.98506	-0.94514
22	0.79349	0.71082	0.33494	0.90203	0.77532	0.40933	-0.52425	-0.4243	0.13186	0.77152	0.92202	0.69035	0.90694	0.86751	0.80019
23							0.82805	-0.11334	-0.90198	-0.52375	-0.78498	0.34162	-0.40095	-0.72884	0.54804
24	0.63513	0.83753	0.33095	0.54046	0.76697	-0.12093	0.72174	0.88202	0.25067	-0.14933	-0.063871	-0.1624	0.94477	0.94266	0.90711
25	-0.86539	-0.89495	-0.51479	-0.87218	-0.82954	-0.71658	-0.038476	-0.59414	-0.33312	-0.82055	-0.45769	0.90464	-0.35932	-0.43575	-0.088087
26	0.16715	0.1487	-0.21275	-0.091364	0.02582	0.47613	0.89974	0.82057	0.47297	0.51913	0.42275	0.57581	0.57159	0.52942	0.69173
27	-0.21848	-0.061897	-0.44085	0.44483	0.26068	0.62716	0.66992	0.60119	0.51842	0.62508	0.66727	0.85524	0.6407	0.68144	0.86402

Cosine value

Good agreement

-1   0   0.5   0.8   1

Fig. 5 Cosine value for all studied **kinematic** simulation specimen responses in continuous hot/cold spectrum. Darker colors represent smaller cosine values, lighter colors cosine values closer to 1

4 to 14 cases showed a similarity value greater than 0.8, with the intervertebral kinematics between L3-L4 showing the least similarity. For the *morphed* configurations, 6 to 16 cases have a cosine value less than 0.5, 10 to 23 cases have a value less than 0.8, and 3 to 16 cases a similarity value greater than 0.8. Also, the intervertebral kinematics between L3 and L4 showed the least concordance for this configuration.

The trend and similarity assessment as a meta-analysis were used for filtering regarding consideration in terms of

injury predictors. Based on that, only the positioned and the morphed configuration were evaluated.

Analysis regarding fracture prediction capabilities

Figure 6 shows exemplarily the stress field map of one specimen in the morphed configuration. Following our recently published analysis approach [23] the area of peak stress in each vertebra at the time of experimental peak force was determined. Therefore, the upper scale limit has been set to 3.5 MPa, the lower bound to 0 MPa for all specimen models in every configuration. The contour plot values were then further filtered until only the elements defining a region of likely fracture were shown. For the specimen that sustained a wedge fracture at L1 classified as a flexion-compression fracture, a stress pressure pattern between T12 and L1 in a triangular shape with highest stresses in the anterior region of L1 becomes visible. The contour plots for all other specimens can be found in the supplementary material; besides flexion-associated fractures, which resulted in wedge or burst fractures, fractures which can be attributed to extension primarily affecting the spinous processes were observed in the experiments.

The contour plots have been rated and classified according to the following criteria: identification of extension or flexion fractures and identification of the fracture region reported in the experiments. Table 1 combines the meta-analysis results for the kinetic data in three categories (good, fair, bad) and the results of the contour plots, i.e., whether the correct fracture mechanism at the position reported in the experimental data is observed in the simulations in color coding. Six out of twenty-six specimen cases detect the fracture type and fracture position in the simulation for the morphed configuration. Ten out of twenty-six cases predicted the fracture type and location reported from the experiments in the positioned configuration. For the morphed configuration, five out of twenty-six cases, the answer of the kinetic evaluation was contradictory to the evaluation of the contour plots. For the positioned configuration, four cases showed conflicting responses.

Discussion

In this study, we investigated the necessary level of individualization of a lumbar spine model in high-dynamic load situations to make a realistic recommendation for potential
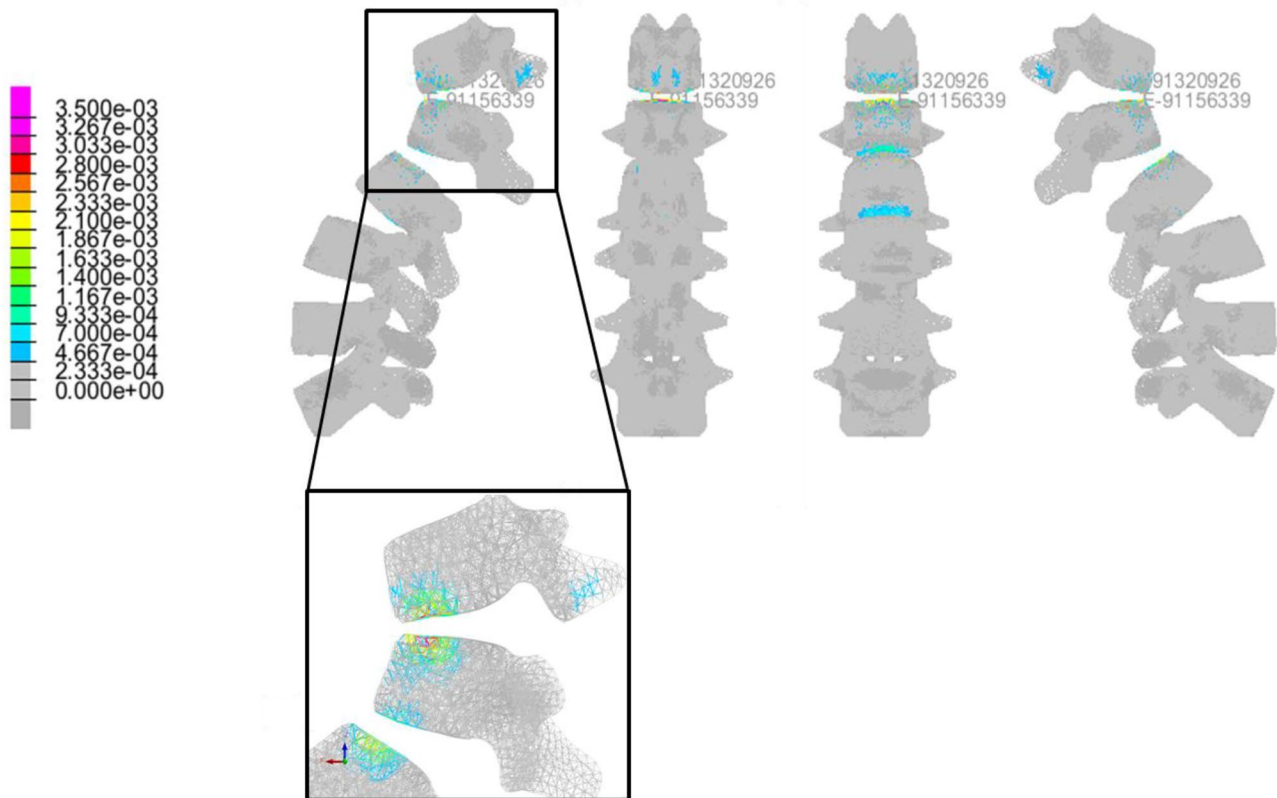
Fig. 6 Finite element model stress field maps (right, rear, front and left side view) of the maximum pressure (negative one third of first invariant) in GPa of the spongiosa of the vertebrae at the moment of peak force exemplarily on one specimen with a wedge fracture at L1. The final step of the filtering is shown and shows how the distribution of pressure is allocated

Table 1 Rating of studied kinetic & kinematic simulation responses vs. experimental response per specimen on a meta level for each configuration. Injury outcomes are color coded (green: injury type and location could be predicted, red: injury type or location were not detected in the contour plots)

Specimens	Kinetic & kinematic rating		
	Morphed	**Positioned**	**Baseline**
1	Fair/good	Good/fair	Bad/bad
3	Good/fair	Fair/bad	Good/bad
4	Good/good	Good/good	Bad/bad
5	Fair/good	Good/fair	Bad/bad
6	Good/fair	Good/fair	Bad/bad
7	Fair/good	Good/good	Bad/bad
8	Good/good	Good/fair	Fair/bad
9	Fair/bad	Fair/bad	Bad/bad
10	Fair/fair	Fair/fair	Bad/bad
11	Bad/bad	Bad/bad	Bad/bad
12	Good/fair	Fair/good	Bad/bad
13	Fair/good	Good/good	Bad/good
14	Fair/good	Fair/good	Bad/fair
15	Fair/bad	Fair/fair	Bad/bad
16	Fair/bad	Good/good	Bad/bad
17	Bad/Bad	Bad/Bad	Fair/fair
18	Fair/fair	Fair/good	Bad/bad
19	Fair/fair	Good/good	Bad/bad
20	Fair/bad	Good/bad	Bad/bad
21	Fair/bad	Good/bad	Bad/bad
22	Fair/fair	Good/fair	Fair/good
23	Fair/bad	Fair/bad	Fair/na
24	Fair/fair	Good/fair	Fair/fair
25	Fair/fair	Fair/bad	Fair/bad
26	Good/bad	Good/bad	Bad/bad
27	Fair/fair	Bad/bad	Bad/bad

Good	Kinematic/kinetic simulation response has same trend & similar magnitude	🟥	Fracture type & location cannot be detected
Fair	Kinematic/kinetic simulation response has same trend	🟩	Fracture type & location can be detected
Bad	Neither trend nor magnitude is met		

application in full-scale load cases. Therefore, three different model types with distinct levels of individualization have been selected, and the effects on the kinematic, kinetic, and fracture prediction capabilities have been analyzed.

Model generation

The experimental test setup was abstracted in the simulation to prevent uncertainties from being introduced into the system by too many modeled parameters. Consequently, the measured accelerations for each specimen were applied to the bottom of the test setup. A point mass on top of the setup and a plate was used to simulate the boundary conditions. However, details influencing the results may have been overlooked by doing so. Also, further integration of experiments and simulation would help to objectify the future modeling of experiments [32, 33].

The base for all levels of individualization within this study is the lumbar spine of THUMS v4.1 developed by Toyota Motor Corporation and Toyota Central R&D Labs. In THUMS v4.1, the musculoskeletal system and the internal organs are modeled in detail based on CT scanning data; the material properties of each tissue are defined to reproduce the PMHS response as given in the literature [34]. However, to apply THUMS v4.1 lumbar spine to a detailed study, the material properties of the intervertebral discs and capsular ligaments were updated according to literature data.

The generic THUMS v4.1 lumbar spine with adapted material was selected as the baseline configuration. The lumbar spine model was globally rotated and integrated into the setup afterward. No individualization adaptions were incorporated into the model for the baseline configuration. This generic configuration aimed to understand how implementing the model into an experimental setup for HBM validation purposes without the exact knowledge of the setup could affect the results. As there were no changes to the intervertebral angles, the lumbar spines' curvature only matches the corresponding X-rays in some instances purely by coincidence.

The exact change of intervertebral angles was used for the next level of individualization, named the positioned configuration. Nevertheless, investigation with angles directly measured from the test data might come to different conclusions. During vertebrae positioning using ANSA, spatial difficulties with the spinal processes of adjacent vertebrae occurred. These were expected as the THUMS v4.1 lumbar spine is based on one individual's lumbar spine; with the positioning, we try to adapt the position to the anthropometry of another specimen.

Nevertheless, the needed adjustments in the x- and z-direction to avoid intersections were minor compared to the applied angles. Finally, the information used for the individualization was only in one plane, i.e., the sagittal plane. Thus, this study did not use information on the position in the frontal plane. As the lumbar spine might not be perfectly symmetrical to the sagittal plane, this second level of information could give further insight into lumbar spine fracture biomechanics. However, compared to the spinal segmental angles measured in the sagittal plane, angles in the frontal plane are smaller in subjects without medical conditions. For the most detailed level of individualization, named morphing, in addition to changing the intervertebral angles, the sagittal heights of the vertebral bodies and intervertebral discs have been measured in the pre-test sagittal X-rays and integrated into the modified THUMS v4.1 model.

This partial individualization does not involve parameters from other planes for several reasons:

1. Lack of imaging data with sufficient quality to determine parameters.
2. Adaption of the THUMS lumbar spine would require a method to complete the parametrization of the model.
3. This study aimed to investigate the lowest needed level of individual parametrization.

Studies investigating the sensitivity of lumbar spine loading to anatomical parameters showed that variations of the vertebral body height, disc height, transverse process width, and the curvature of the lumbar spine are most influential [9, 11]. Therefore, the authors decided to reduce the individualization to a minimum level. The morphing and positioning were performed using ANSA. In cases where the adaptions were too big, ligaments were recreated and re-meshed.

Following previous studies [12], averaged material properties were used for the simulations even though interpersonal variance in material properties might significantly influence simulative responses. Also, visco- and poroelastic behavior of the vertebrae is neglected; this might be important when loading is applied with higher velocities. Finally, articular cartilage was not modeled, possibly influencing the facet joint biomechanics. However, it is deemed that the influence on the relative results between the different initial postures will still be valid in the presence of cartilage.

Specimens with excessive disc height loss, bridging osteophytes, or inconsistent alignment were not included in the study [20], however degeneration can have a major influence on the kinematics and kinetics, and thus, affect the fracture behavior of lumbar vertebrae in physiological loading conditions [35]. Therefore, future studies should use the example Natarajan [36–38] et al. to investigate how degeneration affects highly dynamic loading conditions.

The muscle structures on the specimens for the physical experiments were removed [39], so no muscle activation

was considered in the simulation models. However, it has been shown that muscle activation has an influence on occupant kinematics and thus on the probability of injury in a crash [40]. Therefore, the influence of autochthonous back muscles on fracture risk in the lumbar spine should be further investigated in future studies.

Validation

The models were validated using kinetic and kinematic responses from simulation locations corresponding to the experiment's measurement locations. Failure criteria were not used for validation. Qualitatively, the configuration with the highest degree of individualization showed the closest agreement with the experiments, followed closely by the positioned configuration. At the same time, the baseline configuration performed worst.

The cosine value calculated to quantify the deviation of the simulation response from the experimental data supports this observation (Figs. 3 and 5). Even though the cosine value is an uncommon way to measure the similarity between an experimental and a simulation response, it is frequently used to measure the similarity in text analysis [31], and it satisfies the need to measure the similarity between experiment and simulation quantitively. Commonly used rating metrics are CORA and EEARTH (ISO/TR 16250:2013). However, the parameter customizations possible within these metrics are inherently subjective and have the potential to produce non-trivial scores, which can, in turn, influence the conclusions drawn from a study [41].

The gross biomechanical behavior of the model, as described by the load-time curves (e.g., Fig. 2) and the intervertebral kinematics (e.g., Fig. 4), was not in good agreement with the experimentally determined data for the baseline configuration. The explanation might be that the model's initial position for the baseline configuration was only globally adjusted to the initial position of the specimen in the experiment; previous validation efforts with THUMS v4.1 [42] or THUMS v5 [43] found similar results.

In comparison, the positioned configuration, i.e., the gross biomechanical behavior of the model, as described by the load-time curves (e.g., Fig. 2) and the intervertebral kinematics (e.g., Fig. 4), was in good agreement with the experimentally determined data. This observation is supported by the respective cosine values (Figs. 3 and 5), indicating that the initial position has an influence not only on kinematics but also on kinetics.

At the highest level of individualization, the gross biomechanical behavior of the model, as described by the load-time curves (e.g., Fig. 2) and the intervertebral kinematics (e.g., Fig. 4), was in slightly better agreement compared to positioned data. In this configuration, the vertebral bodies' angular position and the vertebral bodies' height were individualized; the latter, including the wedge angle, i.e., the relation of the anterior height of the vertebral bodies in relation to their posterior height. As described in Section Model Generation, previous studies found an influence of vertebra body height on lumbar spine kinematics. However, these studies only investigated physiological loading conditions, i.e., non-crash-related dynamic loading. Current studies on the Global Human Body Model Consortium (GHBMC) lumbar spine under dynamic loading conditions [44] indicate that the vertebral height might not influence the response of the lumbar spine that much.

Regarding the correlation of between experimental and simulative responses, the third configuration performed better than the second configuration. However, this study aimed to propose a strategy for considering as many details on different spinal anthropometries as possible. The adaption of the heights, combined with the positioning, dramatically increases the number of possible spine models. A viable alternative could be further investigating the relationship between the relative wedging of vertebral bodies and the spinal position [45]. That could allow vertebral wedging and position to be clustered, thus reducing the complexity of the spinal models. Besides, the model setup in configuration 3 is more time-consuming and can lead to model deficiencies, e.g., intersections need to be re-mesh, which would hinder the model's use in the automotive development processes.

Fracture prediction capabilities

Fracture prediction capabilities were evaluated based on previously developed, completely individualized lumbar spine models [23]. The morphed configuration possesses the best fracture prediction properties. The positioned configuration performed slightly worse. Due to the baseline configuration's poor performance in the validation, it was excluded from further evaluation of the fracture prediction capabilities.

The fracture prediction capabilities are rated in Table 1. First, the kinetic and kinematic response agreement to the experiment is classified as either 'good,' 'fair,' or 'bad.' The pressure distribution explains whether a fracture could be predicted and whether the fracture location is met. If the simulative kinematic response does not align with the experimental response, the fracture location cannot be predicted. That indicates a relationship between the kinematics and the location and type of fracture. As the initial posture influences the kinematics, the initial posture directly influences the spinal injury mechanism. Three models show larger pressure areas than others; the reason might be the vertebral body size, which was not adapted in this configuration, and

differences in material properties in the experiment due to sex.

In comparison, the morphed configuration shows a slightly better fracture prediction capability. As an interpersonal variation of the vertebral disc height influences spinal stiffness [12] and disc height was adapted in this configuration, this might be another factor affecting the quality of the fracture prediction. This influence of vertebral disc thickness variation might indicate that the wedging angle influencing the lumbar lordosis has an effect on the spinal response. This hypothesis aligns with previous findings on geometrical personalized finite-element models of lumbar spines [46]. Thus, it is not only the vertebral disc size but also the wedging angle that affects the spinal response [12, 47].

Validation and fracture prediction capabilities draw a similar picture: the morphed configuration performs slightly better than the positioned configuration. However, besides the above arguments regarding fracture prediction capabilities, the positioned models could also predict fractures and the fracture locations. The positioned configuration also slightly overpredicted fractures. If the component load case is abstracted and considered in the full-scale application, it would be preferable to evaluate conservatively using the positioned configuration instead of having a high effort to build a morphed model. Hence, there is support that the positioned configuration is sufficient, for evaluating the performance of safety system for different anthropometries.

However, the study was designed as a pure component load case of the lumbar spine under dynamic compression-flexion. The simulation matrix consisted of two individualization parameters. Future studies could investigate whether completely subject-specific modeling of the lumbar spine improves the kinematic and kinetic responses and injury prediction capabilities. Furthermore, more levels of individualization, including other parameters, could be examined. Moreover, an investigation of how different degrees of customization affect full-scale load cases and a study of the performance under other loading conditions are needed. Finally, the assessment of the fracture prediction capabilities was inherently subjective. Thought should also be given to establish an objective evaluation standard for contour plots.

Conclusions

The main objective of this study was to find the coarsest level of individualization needed to simulate vertebral body fractures to ease full-scale analysis. Therefore, a bottom-up approach was chosen, and three different lumbar spine individualizations were evaluated under dynamic loading. The kinematic and kinetic simulation response was compared to the experimental response for each of the twenty-six

specimens, and the fracture prediction capabilities were rated compared to the injuries observed in the experiment. In conclusion, the models with the highest degree of individualization, i.e., morphing, performed best, followed by the positioned configuration. As the morphing of the vertebra and intervertebral discs heights is very elaborate, it might be challenging to routinely integrate it into full-body models. Focusing on the positioning of vertebral bodies, if full-body models are analyzed for injury reconstruction or prediction, may therefore be a suitable approach.

Authors' contribution statement: Conceptualization: Laura Kathrin Rieger, Steffen Pelschus, Brian Stemper, Methodology: Laura Kathrin Rieger, Steffen Peldschus, Brian Stemper, Formal analysis and investigation: Laura Kathrin Rieger, Writing - original draft preparation: Laura Kathrin Rieger, Writing - review and editing: Steffen Peldschus, Mirko Junge, Rachel Cutlan, Brian Stemper, Funding acquisition: not applicable, Resources: not applicable; Supervision: Brian Stemper, Steffen Peldschus.

Data availability The study protocol was approved by the Subcommittee on Human Studies at the Clement J. Zablocki Veterans Affairs Medical Center in Milwaukee, WI, USA.

Declarations

Ethics approval All lumbar spine specimens for this study were obtained from donors through the Wisconsin Donor Network.

Clinical trial number Not applicable.

Informed consent Consent to participate/consent to publish: Consent for spine donation was obtained from the next of kin.

Conflict of interest The authors do not have any conflict of interest to disclose.

References

1. Leucht P, Fischer K, Muhr G et al (2009) Epidemiology of traumatic spine fractures. Injury 40(2):166–172. https://doi.org/10.1016/j.injury.2008.06.040
2. Pintar FA, Yoganandan N, Maiman DJ et al (2012) Thoracolumbar spine fractures in frontal impact crashes. Ann Adv Automot Med (56): 277–283
3. Wang MC, Pintar FA, Yoganandan N et al (2009) The continued burden of spine fractures after motor vehicle crashes. J Neurosurg Spine 10:86–92. https://doi.org/10.3171/SPI.2008.10.08279
4. Rao RD, Berry CA, Yoganandan N et al (2014) Occupant and crash characteristics in thoracic and lumbar spine injuries

resulting from motor vehicle collisions. Spine J 14(10):2355–2365. https://doi.org/10.1016/j.spinee.2014.01.038

5. Jorlöv S, Bohman K, Larsson A (2017) Seating positions and activities in highly automated cars – a qualitative study of future automated driving scenarios. In: Proceedings of the IRCOBI Conference, pp 13–22

6. Östling M, Jeppsson H, Lubbe N (2019) Predicting crash configurations in passenger car to passenger car crashes to guide the development of future passenger car safety. In: Proceedings of the IRCOBI Conference, pp 626–643

7. Richardson R, Donlon J-P, Jayathirtha M et al (2020) Kinematic and injury response of reclined PMHS in frontal impacts. Stapp Car Crash J 64:83–153. https://doi.org/10.4271/2020-22-0004

8. Kaufman RP, Ching RP, Willis MM et al (2013) Burst fractures of the lumbar spine in frontal crashes. Accid Anal Prev 59:153–163. https://doi.org/10.1016/j.aap.2013.05.023

9. Niemeyer F, Wilke H-J, Schmidt H (2012) Geometry strongly influences the response of numerical models of the lumbar spine–a probabilistic finite element analysis. J Biomech 45(8):1414–1423. https://doi.org/10.1016/j.jbiomech.2012.02.021

10. Thacker BH, Wu Y-T, Nicolella DP et al (1997) Probabilistic injury analysis of the cervical spine. American Institute of Aeronautics and Astronautics, Inc., pp 2093–2103. https://doi.org/10.2514/6.1997-1135

11. Putzer M, Ehrlich I, Rasmussen J et al (2016) Sensitivity of lumbar spine loading to anatomical parameters. J Biomech 49(6):953–958. https://doi.org/10.1016/j.jbiomech.2015.11.003

12. Meijer GJM, Homminga J, Veldhuizen AG et al (2011) Influence of interpersonal geometrical variation on spinal motion segment stiffness: implications for patient-specific modeling. Spine 36(14):929–935. https://doi.org/10.1097/BRS.0b013e3181fd7f7f

13. Izumiyama T, Nishida N, Iwanaga H et al (2018) The analysis of an individual difference in human skeletal alignment in seated posture and occupant behavior using HBMs. In: Proceedings of the IRCOBI Conference, pp 549–560

14. Izumiyama T, Nishida N, Yamagata H et al (2022) Analysis of individual variabilities for lumbar and pelvic alignment in highly reclined seating postures and occupant kinematics in a collision. In: Proceedings of the IRCOBI Conference, pp 941–955

15. Sato F, Miyazaki Y, Morikawa S et al (2021) The effect of seat back inclination on spinal alignment in automotive seating postures. Front Bioeng Biotechnol 9:1–17. https://doi.org/10.3389/fbioe.2021.684043

16. Zhang K, Cao L, Fanta A et al (2017) An automated method to morph finite element whole-body human models with a wide range of stature and body shape for both men and women. J Biomech 60:253–260. https://doi.org/10.1016/j.jbiomech.2017.06.015

17. Beillas P, Berthet F (2017) An investigation of human body model morphing for the assessment of abdomen responses to impact against a population of test subjects. Traffic Inj Prev 18(Suppl 1):142–147. https://doi.org/10.1080/15389588.2017.1307971

18. Shi X, Cao L, Reed MP et al (2014) A statistical human rib cage geometry model accounting for variations by age, sex, stature and body mass index. J Biomech 47(10):2277–2285. https://doi.org/10.1016/j.jbiomech.2014.04.045

19. O'Cain CM, Gepner BD, Spratley EM et al (2019) Pipeline for specimen specific bone-ligament-cartilage finite element models. Proceedings of Ohio State University Injury Biomechanics Symposium: 1–6

20. Stemper BD, Chirvi S, Doan N et al (2018) Biomechanical tolerance of whole lumbar spines in straightened posture subjected to axial acceleration. J Orthop Res 36(6):1747–1756. https://doi.org/10.1002/jor.23826

21. Mattucci SFE, Moulton JA, Chandrashekar N et al (2012) Strain rate dependent properties of younger human cervical spine ligaments. J Mech Behav Biomed Mater 10:216–226. https://doi.org/10.1016/j.jmbbm.2013.04.005

22. Newell N, Carpanen D, Grigoriadis G et al (2019) Material properties of human lumbar intervertebral discs across strain rates. Spine J 19(12):2013–2024. https://doi.org/10.1016/j.spinee.2019.07.012

23. Rieger LK, Shah AS, Schick S et al (2024) Subject-specific geometry of FE lumbar spine models for the replication of fracture locations using dynamic drop tests. Ann Biomed Eng. https://doi.org/10.1007/s10439-023-03402-y

24. Peldschus S, Wagner A, Muehlbauer J et al (2021) Standardised validation procedure for qualifying the HBM to be used for assessing effectiveness of pilot protection principles

25. Armijo-Olivo S, Jara X, Castillo N et al (2006) A comparison of the head and cervical posture between the self-balanced position and the Frankfurt method. J Oral Rehabil 33(3):194–201. https://doi.org/10.1111/j.1365-2842.2005.01554.x

26. Harrison DE, Harrison DD, Cailliet R et al (2000) Cobb Method or Harrison posterior tangent method. Spine 25(16):2072–2078

27. Berthonnaud E, Dimnet J, Roussouly P et al (2005) Analysis of the sagittal balance of the spine and pelvis using shape and orientation parameters. J Spinal Disord Tech 18(1):40–47. https://doi.org/10.1097/01.bsd.0000117542.88865.77

28. Mac-Thiong J-M, Labelle H, Berthonnaud E et al (2007) Sagittal spinopelvic balance in normal children and adolescents. Eur Spine J 16(2):227–234. https://doi.org/10.1007/s00586-005-0013-8

29. Park S-M, Song K-S, Park S-H et al (2015) Does whole-spine lateral radiograph with clavicle positioning reflect the correct cervical sagittal alignment? Eur Spine J 24(1):57–62. https://doi.org/10.1007/s00586-014-3525-2

30. Rocabado M (1983) Biomechanical relationship of the cranial, cervical, and hyoid regions. J Craniomandib Pract 1(3):61–66. https://doi.org/10.1080/07345410.1983.11677834

31. Han J, Kamber M, Pei J (2012) // 2011) Getting to Know Your Data. In: Han J, Kamber M, Pei J (eds) Data Mining. Concepts and techniques, 3. ed. Elsevier; Elsevier Science, Burlington, pp 39–82

32. Anderson AE, Ellis BJ, Weiss JA (2007) Verification, validation and sensitivity studies in computational biomechanics. Comput Methods Biomech Biomed Engin 10(3):171–184. https://doi.org/10.1080/10255840601160484

33. Fuchs T (2018) Objektivierung der Modellbildung von verletzungsmechanischen Experimenten für die Validierung von Finite-Elemente Menschmodellen. Dissertation, Ludwig-Maximilians University Munich

34. Iwamoto M, Kisanuki Y, Watanabe I et al (2002) Development of a finite element model of the Total Human Model for Safety (THUMS) and application to injury reconstruction. In: Proceedings of International Technical Conference on the Enhanced Safety of Vehicles (ESV)

35. Chosa E, Goto K, Totoribe K et al (2004) Analysis of the effect of lumbar spine fusion on the superior adjacent intervertebral disk in the presence of disk degeneration, using the three-dimensional finite element method. J Spin Disord Tech 17(2):134–139. https://doi.org/10.1097/00024720-200404000-00010

36. Natarajan RN, Williams JR, Andersson GBJ (2004) Recent advances in analytical modeling of lumbar disc degeneration. Spine 29(23):2733–2741. https://doi.org/10.1097/01.brs.0000146471.59052.e6

37. Natarajan RN, Williams JR, Andersson GBJ (2006) Modeling changes in intervertebral disc mechanics with degeneration. J Bone Joint Surg Am 88 Suppl 236–40. https://doi.org/10.2106/JBJS.F.00002

38. Ruberté LM, Natarajan RN, Andersson GBJ (2009) Influence of single-level lumbar degenerative disc disease on the behavior of

the adjacent segments–a finite element model study. J Biomech 42(3):341–348. https://doi.org/10.1016/j.jbiomech.2008.11.024

39. Stemper BD, Storvik SG, Yoganandan N et al (2011) A new PMHS model for lumbar spine injuries during vertical acceleration. J Biomech Eng 133(8). https://doi.org/10.1115/1.4004655

40. González-García M, Weber J, Peldschus S (2021) Potential effect of pre-activated muscles under a far-side lateral impact. Traffic Inj Prev 22(Suppl 1):148–152. https://doi.org/10.1080/15389588.2021.1982597

41. Albert DL (2020) Variations in user implementation of the CORA Rating Metric. Stapp Car Crash J 64:1–30. https://doi.org/10.4271/2020-22-0001

42. Rieger LK, Draper D, Shah AS et al (2022) Subject-specific Lumbar Spine Finite Element Model Creation and Validation using Dynamic Compression. In: Proceedings of the IRCOBI Conference, pp 886–887

43. Draper D, Shah AS, Peldschus S et al (2020) Initial validation of a human body model lumbar spine using dynamic compression. In: Proceedings of the IRCOBI Conference, pp 213–214

44. Tushak SK, Paul Donlon J, Gepner BD et al (2022) Failure tolerance of the human lumbar spine in dynamic combined compression and flexion loading. J Biomech 135. https://doi.org/10.1016/j.jbiomech.2022.111051

45. Whitcome KK, Shapiro LJ, Lieberman DE (2007) Fetal load and the evolution of lumbar lordosis in bipedal hominins. Nature 450(7172):1075–1078. https://doi.org/10.1038/nature06342

46. Naserkhaki S, Jaremko JL, El-Rich M (2016) Effects of inter-individual lumbar spine geometry variation on load-sharing: geometrically personalized finite element study. J Biomech 49(13):2909–2917. https://doi.org/10.1016/j.jbiomech.2016.06.032

47. Natarajan RN, Andersson GBJ (1999) The influence of lumbar disc height and cross-sectional area on the mechanical response of the disc to physiologic loading. Spine 24(18):1873–1881